Research Article | Vol. 8, No. 1 | 1 Jan 2017 | BIOMEDICAL OPTICS EXPRESS 38

Biomedical Optics EXPRESS

Stimulus-evoked outer segment changes occur before the hyperpolarization of retinal photoreceptors

YIMING LU,[1] BENQUAN WANG,[1] DAVID R. PEPPERBERG,[2] AND XINCHENG YAO[1,2,*]

[1]*Department of Bioengineering, University of Illinois at Chicago, Chicago, IL 60607, USA*
[2]*Lions of Illinois Eye Research Institute, Department of Ophthalmology and Visual Sciences, University of Illinois at Chicago, Chicago, IL 60612, USA*
[*]*xcy@uic.edu*

Abstract: Transient retinal phototropism (TRP) has been predominantly observed in rod photoreceptors activated by oblique visible light stimulation. Dynamic confocal microscopy and optical coherence tomography (OCT) have revealed rod outer segment (ROS) movement as the physical source of TRP. However, the physiological source of ROS movement is still not well understood. In this study, concurrent near-infrared imaging of TRP and electroretinogram (ERG) measurement of retinal electrophysiology revealed that ROS movement occurs before the onset of the ERG a-wave, which is known to reflect the hyperpolarization of retinal photoreceptors. Moreover, substitution of normal superfusing medium with low-sodium medium reversibly blocked the photoreceptor ERG a-wave, but largely preserved the stimulus-evoked ROS movements. Our experimental results and theoretical analysis indicate that early, disc-based stages of the phototransduction cascade, which occur before the hyperpolarization of retinal photoreceptors, contribute to the TRP associated ROS movement.

OCIS codes: (170.1530) Cell analysis; (170.4470) Ophthalmology; (330.4270) Vision system neurophysiology; (330.5310) Vision - photoreceptors; (330.5370) Physiological optics; (330.5380) Physiology; (330.4595) Optical effects on vision; (330.7331) Vision optics, receptor optics.

References and links

1. R. Lu, A. M. Levy, Q. Zhang, S. J. Pittler, and X. Yao, "Dynamic near-infrared imaging reveals transient phototropic change in retinal rod photoreceptors," J. Biomed. Opt. **18**(10), 106013 (2013).
2. B. Wang, Q. Zhang, R. Lu, Y. Zhi, and X. Yao, "Functional optical coherence tomography reveals transient phototropic change of photoreceptor outer segments," Opt. Lett. **39**(24), 6923–6926 (2014).
3. X. Zhao, D. Thapa, B. Wang, Y. Lu, S. Gai, and X. Yao, "Stimulus-evoked outer segment changes in rod photoreceptors," J. Biomed. Opt. **21**(6), 065006 (2016).
4. W. Stiles and B. Crawford, "The luminous efficiency of rays entering the eye pupil at different points," Proc. R. Soc. Lond., B **112**(778), 428–450 (1933).
5. K. P. Hofmann, R. Uhl, W. Hoffmann, and W. Kreutz, "Measurements on fast light-induced light-scattering and -absorption changes in outer segments of vertebrate light sensitive rod cells," Biophys. Struct. Mech. **2**(1), 61–77 (1976).
6. H. Kühn, N. Bennett, M. Michel-Villaz, and M. Chabre, "Interactions between photoexcited rhodopsin and GTP-binding protein: kinetic and stoichiometric analyses from light-scattering changes," Proc. Natl. Acad. Sci. U.S.A. **78**(11), 6873–6877 (1981).
7. D. R. Pepperberg, M. Kahlert, A. Krause, and K. P. Hofmann, "Photic modulation of a highly sensitive, near-infrared light-scattering signal recorded from intact retinal photoreceptors," Proc. Natl. Acad. Sci. U.S.A. **85**(15), 5531–5535 (1988).
8. M. Kahlert, D. R. Pepperberg, and K. P. Hofmann, "Effect of bleached rhodopsin on signal amplification in rod visual receptors," Nature **345**(6275), 537–539 (1990).
9. K. P. Hofmann, A. Schleicher, D. Emeis, and J. Reichert, "Light-induced axial and radial shrinkage effects and changes of the refractive index in isolated bovine rod outer segments and disc vesicles: physical analysis of near-infrared scattering changes," Biophys. Struct. Mech. **8**(1-2), 67–93 (1981).
10. Q. X. Zhang, R. W. Lu, C. A. Curcio, and X. C. Yao, "In vivo confocal intrinsic optical signal identification of localized retinal dysfunction," Invest. Ophthalmol. Vis. Sci. **53**(13), 8139–8145 (2012).

#275927 http://dx.doi.org/10.1364/BOE.8.000038
Journal © 2017 Received 16 Sep 2016; revised 2 Nov 2016; accepted 9 Nov 2016; published 2 Dec 2016

Biomedical Optics EXPRESS

11. Q. Zhang, R. Lu, B. Wang, J. D. Messinger, C. A. Curcio, and X. Yao, "Functional optical coherence tomography enables in vivo physiological assessment of retinal rod and cone photoreceptors," Sci. Rep. **5**, 9595 (2015).
12. X. Yao and B. Wang, "Intrinsic optical signal imaging of retinal physiology: a review," J. Biomed. Opt. **20**(9), 090901 (2015).
13. J. E. Brown and L. H. Pinto, "Ionic mechanism for the photoreceptor potential of the retina of Bufo marinus," J. Physiol. **236**(3), 575–591 (1974).
14. M. E. Burns and D. A. Baylor, "Activation, deactivation, and adaptation in vertebrate photoreceptor cells," Annu. Rev. Neurosci. **24**(1), 779–805 (2001).
15. T. D. Lamb and E. N. Pugh, Jr., "Phototransduction, dark adaptation, and rhodopsin regeneration the proctor lecture," Invest. Ophthalmol. Vis. Sci. **47**(12), 5137–5152 (2006).
16. X. C. Yao and Y. B. Zhao, "Optical dissection of stimulus-evoked retinal activation," Opt. Express **16**(17), 12446–12459 (2008).
17. H. P. Scholl and E. Zrenner, "Electrophysiology in the investigation of acquired retinal disorders," Surv. Ophthalmol. **45**(1), 29–47 (2000).
18. D. Sun, S. Roth, and M. J. Black, "Secrets of optical flow estimation and their principles," in *Computer Vision and Pattern Recognition (CVPR), 2010 IEEE Conference on*, (IEEE, 2010), 2432–2439.
19. N. Otsu, "A threshold selection method from gray-level histograms," Automatica **11**, 23–27 (1975).
20. Y. G. Li, L. Liu, F. Amthor, and X. C. Yao, "High-speed line-scan confocal imaging of stimulus-evoked intrinsic optical signals in the retina," Opt. Lett. **35**(3), 426–428 (2010).
21. Q. X. Zhang, R. W. Lu, Y. G. Li, and X. C. Yao, "In vivo confocal imaging of fast intrinsic optical signals correlated with frog retinal activation," Opt. Lett. **36**(23), 4692–4694 (2011).
22. Q. X. Zhang, J. Y. Wang, L. Liu, and X. C. Yao, "Microlens array recording of localized retinal responses," Opt. Lett. **35**(22), 3838–3840 (2010).
23. N. Yagi, "Structural changes in rod outer segments of frog and mouse after illumination," Exp. Eye Res. **116**, 395–401 (2013).
24. J. Heller, T. J. Ostwald, and D. Bok, "The osmotic behavior of rod photoreceptor outer segment discs," J. Cell Biol. **48**(3), 633–649 (1971).
25. J. Heller, T. J. Ostwald, and D. Bok, "Effect of illumination on the membrane permeability of rod photoreceptor discs," Biochemistry **9**(25), 4884–4889 (1970).
26. T. M. Vuong, C. Pfister, D. L. Worcester, and M. Chabre, "The transducin cascade is involved in the light-induced structural changes observed by neutron diffraction on retinal rod outer segments," Biophys. J. **52**(4), 587–594 (1987).
27. D. C. Mitchell and B. J. Litman, "Effect of ethanol and osmotic stress on receptor conformation. Reduced water activity amplifies the effect of ethanol on metarhodopsin II formation," J. Biol. Chem. **275**(8), 5355–5360 (2000).
28. H. Asai, T. Chiba, S. Kimura, and M. Takagi, "A light-induced conformational change in rod photoreceptor disc membrane," Exp. Eye Res. **21**(3), 259–267 (1975).
29. E. Hessel, A. Herrmann, P. Müller, P. P. Schnetkamp, and K. P. Hofmann, "The transbilayer distribution of phospholipids in disc membranes is a dynamic equilibrium evidence for rapid flip and flop movement," Eur. J. Biochem. **267**(5), 1473–1483 (2000).
30. Y. Zhi, B. Wang, and X. Yao, "Super-Resolution Scanning Laser Microscopy Based on Virtually Structured Detection," Crit. Rev. Biomed. Eng. **43**(4), 297–322 (2015).
31. Y. Zhi, R. Lu, B. Wang, Q. Zhang, and X. Yao, "Rapid super-resolution line-scanning microscopy through virtually structured detection," Opt. Lett. **40**(8), 1683–1686 (2015).
32. X. C. Yao, R. W. Lu, and B. Q. Wang, "Super-resolution scanning through virtully structured detection," USA Provisional Patent, PCT# 61933987 (2014).
33. B. Wang, R. Lu, Q. Zhang, and X. Yao, "Breaking diffraction limit of lateral resolution in optical coherence tomography," Quant. Imaging Med. Surg. **3**(5), 243–248 (2013).

1. Introduction

Transient retinal phototropism (TRP) has been observed in both amphibian (frog) and mammalian (mouse) retinas illuminated by oblique visible light [1]. High-resolution microscopy revealed that the TRP is dominated by rod photoreceptors. Functional optical coherence tomography (OCT) located the anatomic source to rod outer segment (ROS) [2]. Our recent studies with retina slices, which enable a cross-sectional view of mouse and frog photoreceptors, confirmed the ROS movement as the physical mechanism of TRP [3]. This TRP provides a reasonable explanation for the Stiles–Crawford effect (SCE) [4] being predominantly observed in cones and not rods. In other words, the loss of luminous efficiency caused by oblique stimulation may be compensated by the phototropic movement of ROSs.

Although the stimulus-evoked property of TRP indicates a cause-and-effect relationship between phototransduction and TRP, the physiological mechanism underlying TRP remains

Biomedical Optics EXPRESS

unclear. Previous studies of isolated ROS [5, 6] and of isolated intact retina [7, 8] have shown that in response to a visible flash, photoreceptors exhibit an intrinsic near infrared scattering signal. As the ROS movement represents a morphological change in the retina, it is logical to hypothesize that the phototropic response of ROSs is a key component of the light-scattering signal [9], i.e., TRP may also originate from the ROSs. Our previous studies showed that the onset time of the intrinsic optical signal (IOS) precedes the onset time of the electroretinographic (ERG) a-wave, which reflects the hyperpolarization of photoreceptor outer segments (OS) [10, 11], and the rod dominant phototropism was suggested to be a primary contributor to the IOS [1, 12]. Therefore, we further hypothesized that the onset of TRP occurs earlier than cell hyperpolarization in the phototransduction cascade.

To investigate the physiological origin of TRP, we have employed a modified Ringer's medium with sodium ions substituted by choline to maintain a condition of shut-off of rod circulating current and, thus, of suppressed stimulus-evoked hyperpolarization of the rods and signal transmission to downstream neurons (e.g., bipolar cells) [13–15]. Choline-substituted medium achieves the shut-off of the circulating dark current because choline, unlike sodium, does not pass through cyclic guanosine monophosphate (cGMP) gated ion channels. Thus, if TRP has a receptoral origin, it should persist during superfusion with low-sodium medium. Furthermore, the TRP, if resulting from receptoral events upstream from the closure of cGMP-gated ion channels, might develop on a time scale faster than that of the ERG a-wave, which largely reflects the decrease in circulating current through cGMP-gated ion channels.

2. Materials and methods

2.1 Retinal preparation

Both leopard frogs (Rana Pipiens) and mice (Mus musculus) have been used to demonstrate stimulus evoked ROS movement [3]. We selected frog retinas for this study because frog photoreceptors are relatively large and allow unambiguous observation of individual photoreceptors. Therefore, quantitative analysis of ROS movement can be readily implemented. The retinal preparation procedure has been reported in our previous publications [16]. Briefly, leopard frogs were euthanized by decapitation followed by double-pithing after dark adaptation for more than eight hours. The eyes were then enucleated and hemisected along the equator with fine scissors. A circular section of the retina with a diameter of about 6 mm was separated from the retinal pigment epithelium (RPE) and isolated from the back of the eye. Next, the isolated retina was positioned in a chamber (Fig. 1A) with the OS of the photoreceptor facing upward and was continuously superfused with oxygenated Ringer's medium at room temperature (18~20 °C). The Ringer's medium contained 110.0 mM NaCl, 2.5 mM KCl, 1.6 mM $MgCl_2$, 1.0 mM $CaCl_2$, 22.0 mM $NaHCO_3$, and 10.0 mM D-glucose, pH 7.3~7.4. The low-sodium medium was prepared by replacing the NaCl in the Ringer's medium with 110.0 mM choline chloride [7]. All procedures for preparation and study of the retina were performed in a dark room with dim red light illumination. All experiments were performed following the protocols approved by the Animal Care Committee (ACC) at the University of Illinois at Chicago, and conformed to the statement on the use of animals in ophthalmic and vision research, established by the Association for Research in Vision and Ophthalmology (ARVO).

2.2 System setup

As shown in Fig. 1(A), the imaging system was based on a modified NIR light microscope (BX531WI, Olympus, Japan) with a 40X water immersion objective lens (UMPLFLN40XW, NA 0.8, Olympus, Japan). A CCD camera (pixel size: 7.4 μm × 7.4 μm; Pike, Allied Vision, Exton, PA) was employed for image acquisition. The acquisition rate was set to 100 frames per second (fps) with a frame resolution of 400 × 400 pixels. To specify the onset time of ROS movements, the CCD camera was replaced by a CMOS camera (pixel size: 6.5 μm × 6.5

Biomedical Optics EXPRESS

μm; Neo 5.5, Andor Technology Ltd, Belfast, Ireland), providing an acquisition rate of 500 fps with a frame resolution of 431 × 122 pixels. A fiber-coupled light emitting diode (LED) with a central wavelength at 550 nm (bandwidth: ~200 nm) was connected to the microscope to provide oblique light stimulation (angle: ~20°, Fig. 1(B)). The stimulus pattern projected onto the retina was a rectangular area (Figs. 1(B) and 2(A)) of dimensions 19.8 μm × 252 μm that covered about two rod photoreceptors in the lateral direction. The stimulus intensity was empirically set to ~1.13×10^8 photon/μm^2/s to enable robust ROS movement.

Full-field ERG recording [17] was implemented by placing differential electrodes on the top and bottom of the retina (Fig. 1(A), dashed square). The recorded ERG signal (sampling rate: 10 kHz) was processed by a physiological amplifier (DAM 50, World Precision Instruments, Sarasota, FL) with a gain of 1,000 and a bandpass of 0.1 Hz to 10 kHz. The amplified ERG response was digitized using a 16-bit DAQ card (NI PCIe-6351, National Instruments, TX) and was sent to the computer for display and storage. The image acquisition, stimulation and ERG recording were hardware-synchronized and software-controlled by a custom-designed Labview (National Instrument, TX) program.

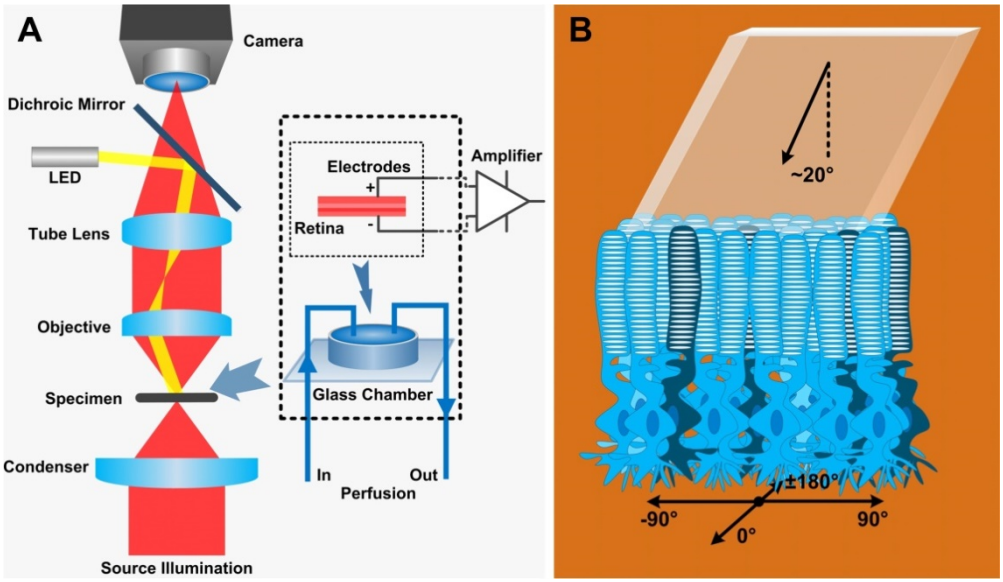

Fig. 1. (A) Schematic diagram of the experiment setup. Left: A custom modified microscope with a 40X water immersion microscope and a CCD (100 fps) or a CMOS (500 fps) camera was employed for imaging. Right: The ERG recoding was achieved by placing electrodes on the retina in a glass chamber (dashed square). The isolated retina was continuously superfused with physiological medium during the experiment. (B) The retina was placed with photoreceptor layer on the top and was obliquely (~20°) stimulated by visible light from the top [2]. The coordinate axes shown at the bottom were used to define the direction of ROS movement. The 90° direction represents ROS movement toward the incident stimulation.

2.3 Experimental procedure

To investigate retinal physiological responses, the retina was consecutively superfused with Ringer's solution, low-sodium solution and then Ringer's solution again. Each superfusion period lasted 20 minutes, allowing a complete replacement of the previous superfusion medium and sufficient retinal recovery, and was followed by a five-second imaging period. During the imaging period, the superfusion was suspended to provide a static imaging environment. Each imaging period was composed of three phases, including a 1.0-s pre-stimulus phase, a 1.0-s stimulus phase and a 3.0-s post-stimulus phase.

Biomedical Optics EXPRESS

2.4 Data analysis

The methods employed for the quantification of ROS movements and the segmentation of active areas were as described previously [2]. An optical flow algorithm [18] was employed to generate a movement magnitude map (Figs. 2(B) and 2(D)) and a movement direction map (Fig. 2(E)) for each acquired retinal image. Based on the magnitude map, a threshold was automatically calculated using Otsu's method [19]. Those pixels that had a higher movement magnitude than the threshold constituted active areas and the rest were inactive areas. The inactive areas on the direction map were then set to blue to highlight the active areas.

The temporal dynamics of the ROS movement magnitude was investigated by calculating the time course of the mean movement magnitude of the ROSs in each frame. The calculation of the mean movement magnitude was similar to that previously used for the computation of IOSs [10, 11]. The primary procedures were the following: a 3-δ threshold and a temporal window were applied to exclude potential spatial and temporal noise contributions. For the 3-δ threshold, a pixel (*p*) with coordinator index $\left(x_p, y_p\right)$ on a magnitude map with frame index *k* was assumed to reflect the signal if its intensity $I_k\left(x_p, y_p\right)$ satisfied

$$I_k\left(x_p, y_p\right) > \bar{I}_{pre}\left(x_p, y_p\right) + 3\delta_{pre}\left(x_p, y_p\right) \tag{1}$$

where $\bar{I}_{pre}\left(x_p, y_p\right)$ represents the mean intensity of the pixels with same index $\left(x_p, y_p\right)$ in all pre-stimulus magnitude maps and $\delta_{pre}\left(x_p, y_p\right)$ represents the standard deviation. The temporal window was further employed to eliminate random movements that may have had higher magnitudes than the 3-δ threshold but were not stimulus-related in magnitude map *k*. That is, we used this temporal window to examine whether $I_{k+1}\left(x_p, y_p\right), \cdots, I_{k+n}\left(x_p, y_p\right)$ were consistently above the 3-δ threshold and *n* was the frame number within the temporal window. Finally, a mean ROS movement magnitude, representing an overall movement level in frame *k*, was calculated by averaging all $I_k\left(x, y\right)$ s that, by the above criterion, were taken to be ROS movement signals, and a magnitude-time curve (Fig. 2(F)) was obtained by aligning the mean ROS movement magnitudes together according to the time sequence.

Biomedical Optics EXPRESS

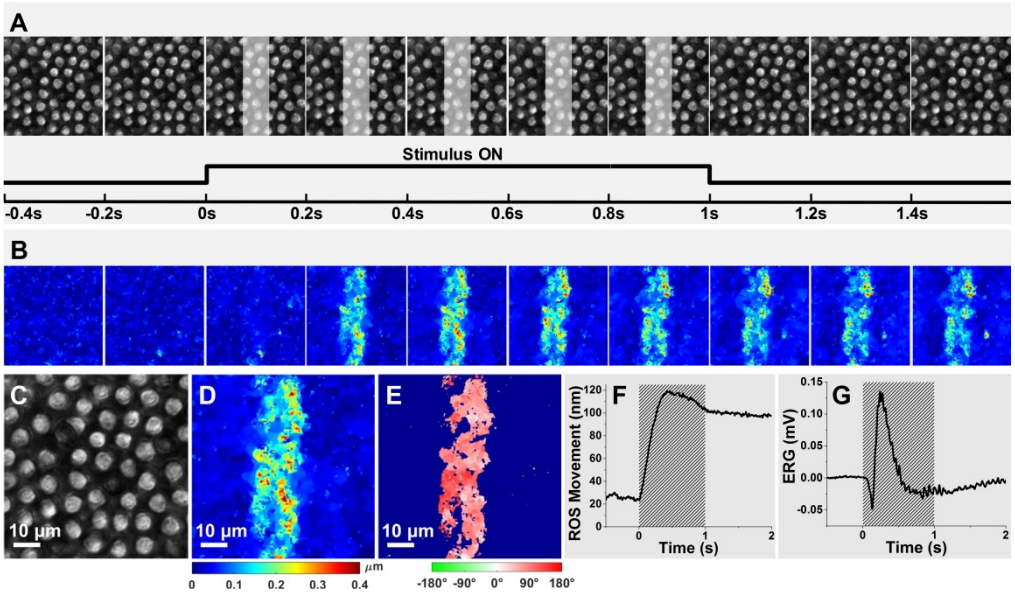

Fig. 2. (A) Top: Representative microscopy images of ROSs acquired in intervals of 0.2 s. The white regions in the panels represent the stimulus pattern presentations. Bottom: The imaging period (5 s) had three phases: pre-stimulus (1 s), stimulus (1 s), and post-stimulus (3 s) phases. (B) Dynamic magnitude changes of ROS movements corresponding to the retinal images in A. Enlarged microscopy image of ROSs acquired at time 0.4 s (C) and the corresponding movement magnitude (D) and direction (E) maps. (F) Time course of the mean magnitude of ROS movements. (G) Full-field ERG recorded from the isolated retina. The shaded areas in F and G indicate the stimulus duration.

3. Results

Figure 2 shows imaging data (Figs. 2(A)-2(E)), and time courses of stimulus-evoked ROS movement (Fig. 2(F)) and the ERG response (Fig. 2(G)) obtained in a representative experiment. This experiment involved superfusion only with normal Ringer's solution, and an image acquisition rate of 100 fps. The Fig. 2(A) images show the mosaic pattern of ROS. The Fig. 2(A) images were obtained before, during and after a 1-s stimulus, and Fig. 2(C) shows replicates, at higher magnification, the image obtained at time 0.4 s. The Fig. 2(B) data show, in color-coded fashion, the image by image determination of ROS movement for the Fig. 2(A) images. The Fig. 2(B) ROS movement image obtained at time 0.4 s, and the color key that applies to the Fig. 2(B) data are shown in Fig. 2(D). The color-coded Fig. 2(E) image shows the direction of ROS movement corresponding to the Fig. 2(D) image. As shown respectively in Figs. 2(F) and 2(G), the stimulus evoked a rapidly rising mean movement of the ROS, and an ERG response that contained a negative going a-wave followed by a positive going b-wave.

A key objective of this study was to investigate the relative times of onset of the stimulus-evoked ROS movement and development of the ERG a-wave. Figure 3, which shows results obtained from a single representative retina, addresses this topic of relative timing of the ROS movement and the ERG a-wave response. To compare the time courses of these responses with an imaging temporal resolution exceeding that of Fig. 2 experiment, the imaging field in the Fig. 3 experiment was confined to a smaller area (Fig. 3(A)) of ROSs, allowing a higher image acquisition rate (500 fps), i.e., a 2-ms temporal resolution. Signal denoising was performed by averaging the magnitude-time curves of ROS movements and ERGs acquired from ten different locations of the retina. Figs. 3(B1) and 3(C1) display the averaged magnitude of ROS movements and ERGs over time. Figs. 3(B2) and 3(C2) provide enlarged illustration for the dashed squares in Figs. 3(B1) and 3(C1), respectively. For the ROS

Biomedical Optics EXPRESS

movements, the corresponding time of the first frame that had a mean movement magnitude larger than the 3-δ threshold (mean plus three standard deviations) was assumed to be the onset time. The criterion also applied for estimating the onset time of the ERG a-wave. The onset times (red triangles in Figs. 3(B2) and 3(C2)) of ROS movements and ERGs were 10 ms and 38 ms, respectively, indicating a 28-ms delay for ERG a-wave onset.

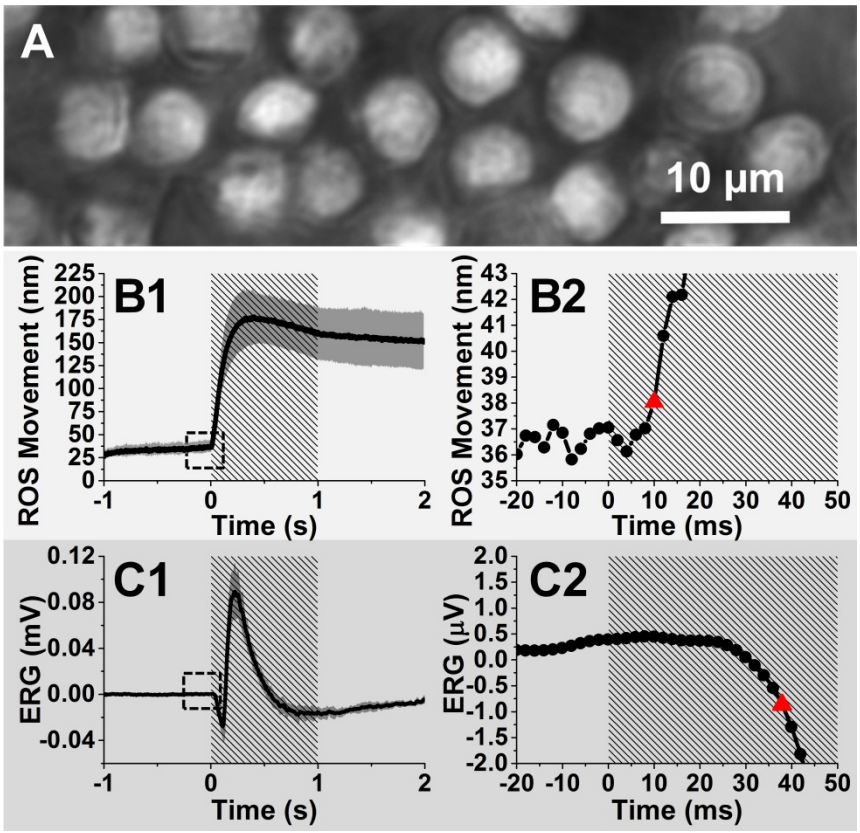

Fig. 3. (A) Representative ROS image acquired at a frame speed of 500 fps. Time course of the averaged mean movement magnitudes of ROSs (B1), and averaged ERGs (C1) acquired from ten different retinal locations. (B2) Enlarged picture of the dashed square in B1. (C2) Enlarged picture of the dashed square in C1. The red triangles in B2 and C2 indicate the onset times determined by the 3-δ threshold of ROS movement and ERG a-wave, respectively. Each data point shown in C2 (sampling rate of the original data: 10 kHz) represents the value exhibited at the end of a given 2-ms interval. Gray areas in B1 and C1 show standard deviations. Shaded areas in B1, B2, C1, and C2 represent stimulation periods.

In order to further investigate the relationship between the stimulus-evoked ROS movement and the electrophysiological response, we conducted comparative experiments with the retinas superfused with control Ringer's medium and low-sodium medium. During the experiment, the imaging area was fixed on the same location of the retina (Figs. 4(A1), 4(B1) and 4(C1)), avoiding possible differences in retinal responses caused by different retinal locations. Retinal images acquired at time 0.4 s (when ROSs usually have the maximum displacement) and their corresponding photoreceptor movement magnitude maps and direction maps are shown in Figs. 4(A1)-4(A3), 4(B1)-4(B3) and 4(C1)-4(C3), respectively.

As shown in Figs. 4(A2), 4(B2) and 4(C2), robust ROS movements were observed in the retina superfused with both normal medium and low-sodium medium. At the same time, the movement direction was centered near 90° (Figs. 4(A3), 4(B3) and 4(C3)), showing that the

Biomedical Optics EXPRESS

stimulated rod photoreceptors swung toward the direction of the stimulus. The coordinates of the movement angle are shown in Fig. 1(B).

Figs 4(A4), 4(B4) and 4(C4) show time courses of the magnitude values of ROS movements. The waveforms of all three panels exhibited a stable and flat stage prior to flash presentation, a rapid rise upon the initiation of the flash stimulus, and a peak value at about 0.5 s.

As illustrated in Figs. 4(A4), 4(B4) and 4(C4), substitution of low-sodium medium did not substantially affect either the time course or the peak amplitude of the ROS movement period. However, the ERG responses were totally abolished by low-sodium medium (Fig. 4(B5)) and recovered essentially fully upon return of normal medium (Fig. 4(C5)).

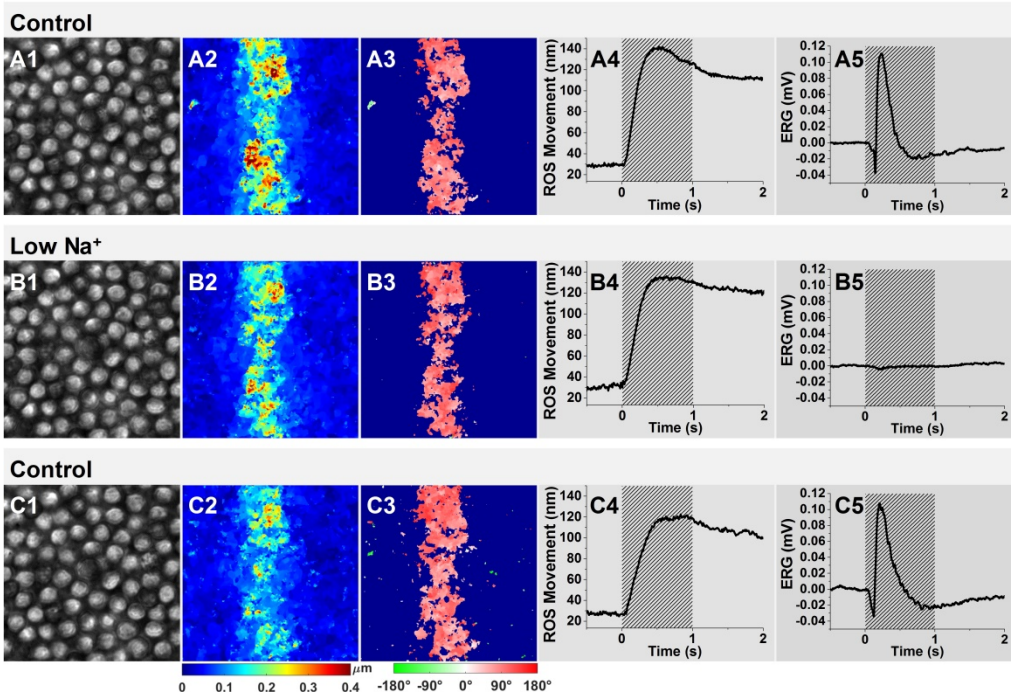

Fig. 4. Comparison of ROS movements and ERGs between control groups (superfusion with Ringer's medium) and the low-sodium group (superfusion with low-sodium medium). The retina superfusion followed a sequence of Ringer's medium superfusion (control group), low-sodium medium superfusion (low Na^+ group), and Ringer's medium superfusion (control group). Representative ROS images acquired from the same area of the retina before (A1), during (B1) and after (C1) superfusion with the low-sodium medium. Representative movement magnitude maps and movement direction maps, before (A2, A3, respectively), during (B2, B3, respectively) and after (C2, C3, respectively) superfusion with the low-sodium medium. Time course of the mean movement magnitude of ROSs and ERGs acquired before (A4, A5, respectively), during (B4, B5, respectively) and after (C4, C5, respectively) the low-sodium superfusion. The magnitude maps (A2, B2 and C2) and direction maps (A3, B3 and C3) were calculated from the retinal images acquired at 0.4 s after the onset of the stimulus in the different groups.

Figure 5 illustrates ROS movement and ERG data obtained from a group of six retinas, including the retina described in Fig. 4. In each panel of Fig. 5, the mean ROS movement or ERG trace (black waveform) is accompanied by the standard deviations of data about the mean (gray areas). For the ROS movement data as well as the ERG data, the relationship of the standard deviation amplitudes to the mean waveform indicates general similarity of the results obtained from different retinas.

Biomedical Optics EXPRESS

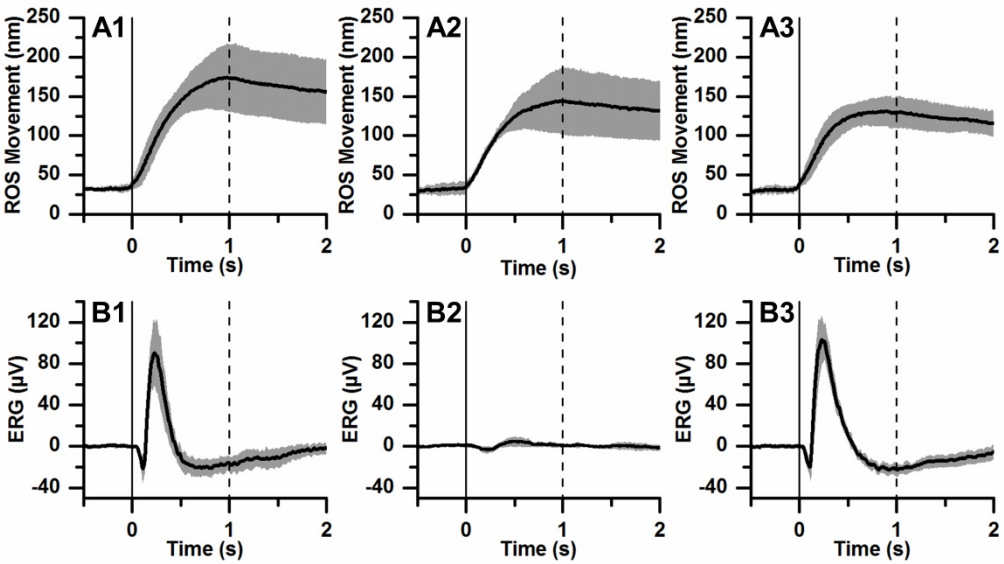

Fig. 5. Averaged ROS movements (A) and ERGs (B) of control (A1, B1), low-sodium (A2, B2), and recovery (A3, B3) groups. Each trace is the average of data obtained from 6 frog retinas. The gray area that accompanies each trace illustrates standard deviation. Vertical solid and dashed lines show stimulus onset and offset, respectively.

4. Discussion

In this study, we have investigated the relationship between the stimulus-evoked ROS movement and the ERG a-wave. In the presence of normal Ringer's solution, we found that the onset of ROS movement occurs earlier (~28 ms) than the onset of the ERG a-wave response (Fig. 3). We hypothesized that ROS movement is driven by signals/processes in the photoreceptors that are upstream from light-induced closure of the photoreceptor cGMP-gated ion channels. To test this hypothesis, we measured the effect of treatment with low-sodium medium, a condition that suppresses ERG a-wave generation. As shown in Figs. 4 and 5, our findings that the low-sodium treatment largely preserves both the peak amplitude and time course of ROS movement provide strong evidence that the events underlying ROS movement do not depend on cGMP-gated ion channel closure. Rather, these events are tied directly or indirectly to the upstream, disc-based phototransduction steps that involve the sequential activation of rhodopsin, transducin and cGMP phosphodiesterase (PDE). As shown in Figs. 4 and 5, we observed that superfusion with low-sodium medium has little or no effect on the onset time of the ROS movement response. This observation argues against an effect of channel closure (i.e. ERG a-wave development) in either accelerating or delaying initiation of the ROS movement. An earlier study, employing OCT to characterize IOSs in the intact eye of frog, showed that onset of the stimulus-evoked IOS response can occur as early as 4 ms after flash initiation (Fig. 4C in [11]). This interval is shorter than the 10-ms onset time determined for ROS movement in the present work. Because the previous and present studies differ in several respects, including the investigation of intact eye vs. isolated retina, OCT vs. microscopy system, and possible differences in photo stimulation efficiency, the extent to which the presently measured ROS movement accounts for the previously measured overall IOS remains to be determined. For isolated retina, this issue can be addressed in future work by using either a camera with higher frame acquisition rate, or other high-speed imaging techniques such as high-speed confocal [10, 20–22] or OCT [2, 11] systems.

It is interesting to consider our data in the context of the possibility that the blockage of rod circulating current can provide osmotic and therefore structural changes within the photoreceptor [23, 24]. The preservation of stimulus-evoked ROS movement in low-sodium

Biomedical Optics EXPRESS

medium argues against the possibility that an osmotic change tied to a light-induced change in closure of cGMP-gated ion channels underlies the ROS response. However, remaining open possibilities include stimulus-evoked rhodopsin-, transducin-, and/or PDE-dependent permeability changes [25–27], compression of disc membranes [28], and the distribution of the phospholipids in the disc membranes [29]. As TRP clearly depends on a structural perturbation of the OS, these possibilities offer possible avenues for investigating the basis of TRP at a subcellular level.

This study has involved the recording of stimulus-evoked retinal responses from isolated retina. We selected isolated retina as the experimental preparation for two reasons. First, isolated retina (in comparison with eyecup preparation or intact eyes) allows a more precise and efficient control of the bathing environment. Second, the free distal ends of ROSs, realized by separation of the retina from the RPE, enable a direct view of, and facile quantification of, the ROS movements. However, it is important to clarify that the movement magnitude of the photoreceptors in the isolated retina may differ from that in the natural condition in which the ROSs interface with the RPE. For pursuing *in vivo* investigation, we are constructing a super-resolution ophthalmoscope, based on virtually structured detection (VSD) [30–33].

5. Conclusion

This study reports a comparative investigation of TRP associated ROS movement and electrophysiological dynamics in the retina stimulated by oblique visible light. Our experimental results and theoretical analysis suggest that early, disc-based stages of the phototransduction cascade, which occur before hyperpolarization, contribute to the TRP-associated movement of rod photoreceptors. As TRP reflects a functional response of the retina to a light stimulus, further study of the TRP mechanism will not only benefit in depth understanding of photoreceptor physiology, but also may provide a valuable biomarker for advanced diagnosis of retinal diseases.

Acknowledgment

The authors thank Professor Klaus Peter Hofmann for his helpful comments on this manuscript, and Mr. Marek T. Mori for mechanical design and manufacturing. This research was supported in part by NIH grants R01 EY023522, R01 EY024628, P30 EY001792, and R21 EY023430; by NSF grant CBET-1055889; by Research to Prevent Blindness (New York, NY); and by the Daniel F. and Ada L. Rice Foundation (Skokie, IL).